A Delay Filter for an ir-UWB Front-End

Sumit Bagga, Sandro A. P. Haddad, Wouter A. Serdijn, John R. Long and Erik B. Busking

***Abstract*—A continuous-time analog delay is designed as a requirement for the autocorrelation function in the Quadrature Downconversion Autocorrelation Receiver (QDAR) [1]. An eight-order Padé approximation of its transfer function is selected to implement this delay. Subsequently, the orthonormal form [1] is adopted, which is intrinsically semi-optimized for dynamic range, has low sensitivity to component mismatch, high sparsity and whose coefficients can be physically implemented. Each coefficient in the state-space description of the orthonormal ladder filter is implemented at circuit level using a novel 2-stage gm cell employing negative feedback. Simulation results in IBM's Bi-CMOS 0.12 µm technology show that this delay filter requires a total current of 70 mA at a 1.6 V power supply. The 1-dB compression point of the delay is at 565 mV and the SNR is 47.5 dB. On performing a Monte Carlo simulation it becomes evident that the response of the frequency selective analog delay does not suffer drastically from neither process variations nor component mismatch.**

***Index Terms*—analog delay, filter, low power, quadrature downconversion autocorrelation receiver, state-space description, impulse radio, ultra-wideband**

I. INTRODUCTION

Although impulse radio ultra-wideband technology promises enhanced data throughput with low-power consumption, it inseparably introduces several challenging design issues. Ultra-wideband systems transmit at very low spectral densities and occupy a large amount of bandwidth, thus it is unequivocal that interference introduced from neighboring narrowband systems is a serious predicament, which could severely hamper or even degrade the overall performance of the system.

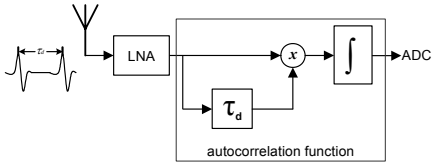

Fig. 1. Transmit reference scheme by Hoctor and Tomlinson

In the transmit reference scheme proposed by Hoctor and Tomlinson [2] (see Fig. 1), consecutive pulses are transmitted with a predefined delay τ_d between them. The first pulse acts as a reference, whereas the second pulse is modulated. The autocorrelation receiver correlates the incoming signal with a delayed version of the previous signal. The absolute value of the output after integration is in fact the energy of the pulse while the polarity of the output contains the data.

A *Quadrature Downconversion Autocorrelation Receiver (QDAR)* (see Fig. 2) [1] is designed to operate in the presence of strong narrowband interference, while still being able to detect the incoming UWB signal.

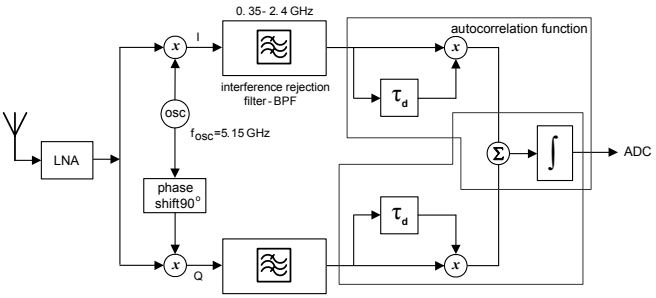

Fig. 2. Quadrature downconversion autocorrelation receiver

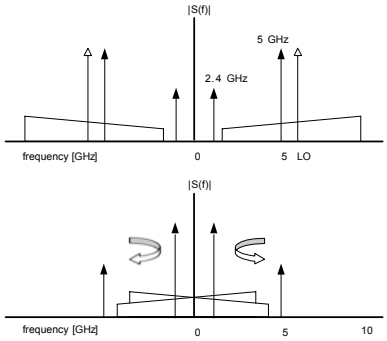

Fig. 3. Frequency spectrum before (top) downconversion and after (bottom) downconversion

The QDAR works on the principle of frequency wrapping; it folds the ultra-wideband frequency spectrum around the origin. At the same time, the narrowband interferers at 5.5 and 2.4 GHz are positioned outside the band of interest and are simply removed by the means of a band-pass filter (see Fig. 3). Besides resolving the issues of synchronization and capturing multipath energy, the QDAR exploits the fact that detection with an autocorrelation receiver is feasible as long as the relative polarity and shape of consecutive pulses is preserved.

In regards to the transmit reference scheme and from an implementation point of view, one is drawn to the conclusion that the bottleneck to this concept is the physical realization of an accurate continuous-time delay required to execute the autocorrelation function at high frequencies.

S. Bagga, S. A. P. Haddad, Wouter A. Serdijn and John R. Long are with the Electronics Research Laboratory, Faculty of Electrical Engineering, Mathematics and Computer Science, Delft University of Technology, Mekelweg 4, 2628CD, Delft, The Netherlands (e-mail: {s.bagga, s.haddad, w.a.serdijn, j.r.long}@ewi.tudelft.nl).

Erik B. Busking is with TNO, Defence, Security and Safety, P.O. Box 96864, 2509JG The Hague, The Netherlands (e-mail: erik.busking@tno.nl).

0-7803-9398-8/05/$20.00 ©2005 IEEE

In this paper we propose a frequency selective analog time delay. A system analysis is performed in Section 2. Section 3 discusses the transformation procedure of the transfer function of the delay into the orthonormal state-space form. Transconductance amplifiers are frequently employed in filters designed for high-frequency applications and are thus also in this particular case of impulse radio ultra-wideband circuit design. Section 4 describes the design and implementation of the 2-stage negative feedback transconductance cell. Simulation data of the transconductance amplifier as well as the overall delay performance are given in Section 5. Section 6 presents the conclusions.

II. SYSTEM ANALYSIS

An eighth order band-pass filter with a pass-band attenuation of 20 dB was designed in [3] to remove the narrowband interferers. However, as the interferers are stronger than the UWB signal their presence after downconversion and filtering may still deteriorate the outcome of the autocorrelation function. Hence, to further reduce the influence of the narrowband interferers, frequency selectivity is introduced in the delay element as illustrated in Fig. 4.

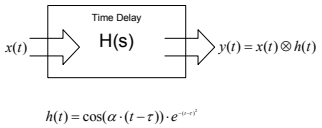

Fig. 4. Filter based time delay for a QDAR.

Assuming that the incoming waveform at the receiver, *x(t)*, is a Morlet given by,

$$x(t) = \cos(\alpha \cdot (t-\tau)) \cdot e^{-(t-\tau)^2} \tag{1}$$

where α is the center frequency and τ is the time instant at which the Morlet waveform is centered, the impulse response, *h(t)*, of the delay filter is chosen to ***match*** the incoming signal (i.e. *h(t)=x(t)*) and therefore the output of the time delay, *y(t)*, is the convolution of the incoming signal and the impulse response of the filter, given by,

$$y(t) = \int_0^t \cos(\alpha \cdot (\tau_1 - \tau)) \cdot e^{-(\tau_1-\tau)^2} \cdot \cos(\alpha \cdot (t-\tau_1-\tau)) \cdot e^{-(t-\tau_1-\tau)^2} d\tau_1 \tag{2}$$

After simplifying (2), one obtains,

$$y(t) = \beta \cdot \cos(\alpha \cdot (t-\tau_1-2\tau)) \cdot e^{-0.5\tau(t-2\tau)^2} \tag{3}$$

where β is the gain factor of the convolved waveform.

On comparing (1) with (2), one sees the distinct resemblance between the convolved waveform and the incoming Morlet signal. Through convolution, the Morlet signal is delayed (see Fig. 5.) by a time period equal to τ.

To quantitatively comprehend the effect of gain factor (β) seen in the convolved waveform to the overall performance of the autocorrelation function, the autocorrelation coefficient is calculated, defined as,

$$\rho = \frac{\int_{t1}^{t2} |Em \cdot Ecm|^2 dt}{\sqrt{\int_{t1}^{t2} |Em|^2 dt \cdot \int_{t1}^{t2} |Ecm|^2 dt}} \tag{4}$$

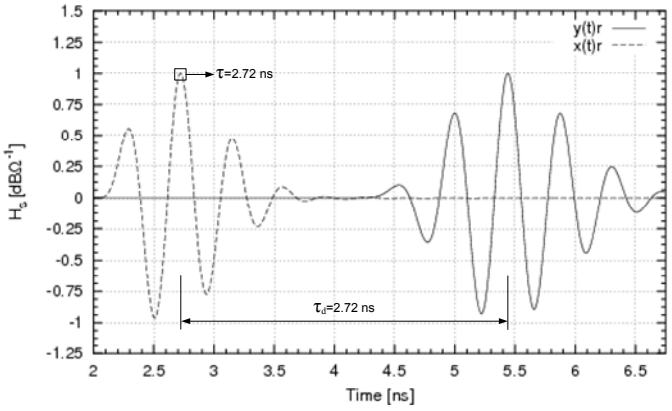

Fig. 5. Normalized input Morlet (left) and output convolved (right) waveforms, respectively.

where E_m and E_{cm} are the respective energy contents of the incoming Morlet waveform and the convolved output waveform, ρ is the autocorrelation coefficient and t_1, t_2 represent the integration time. The parameter ρ is a measure of the error in the autocorrelation. If β were to vary between 0.1-0.9, ρ would change by only 0.01 %, which is in fact negligible. Hence, gain variations do not affect the outcome of the autocorrelation function.

III. SYSTEM DESIGN

A. Transfer function and state-space synthesis

The analysis in [4] showed that, after downconversion, the interferers move adjacent to the band of interest. The interferer (802.11g) at 5.5 GHz appears below 350 MHz and the interferer (802.11b) at 2.4 GHz beyond 3.1 GHz, when down-converting with an oscillator frequency of 5.5 GHz. Note, band-pass filters are introduced after downconversion to minimize the influence of these narrowband interferers. The resulting band of interest is from 0.35-2.6 GHz.

Trade-offs between slope, attenuation and circuit complexity are taken into consideration prior to choosing the filter order of the time delay. An eighth order filter is chosen with 20 dB attenuation. The transfer function (see below) of the filter used as a frequency selective time delay is generated using a Padé approximation [1]. The magnitude transfer as well as the phase response corresponds to that of a Morlet.

$$H(s) = \left[\frac{6.746s^7 - 1.204e17s^6 + 1.375e30s^5 - 2.138e40s^4 + 2.266e51s^3 + 1.361e61s^2 - 4.355e70s + 1.22e82}{s^8 + 4.704e10s^7 + 4.26e21s^6 + 1.276e32s^5 + 5.71e42s^4 + 1.057e53s^3 + 2.861e63s^2 + 2.651e73s + 4.368e83} \right]$$

Once the desired transfer function is formulated, its state-space description is then determined. A state-space description for a given transfer function is not unique, meaning that many state-space descriptions can implement the same transfer function. Moreover, a state-space description of any filter transfer function should be optimized for dynamic range, sensitivity, sparsity and the coefficient values [1], [5].

B. Orthononormal ladder structure

Among known standard state-space descriptions, such as the canonical, the diagonal and the modal, the orthonormal ladder form is notable since it is by definition semi-optimized for dynamic range due to the specific structure of the matrices. Furthermore, since it is derived from a ladder structure, it is intrinsically less sensitive and the matrices are highly sparse. A detailed explanation of the procedure to derive the orthonormal ladder form can be found in [6].

With a state-space approach, the filter can be optimized for dynamic range, sensitivity, sparsity and coefficient values. A low sensitivity suppresses the effect of component variations on the transfer function. It can be proved that a filter that is optimized for dynamic range is also optimized for sensitivity [7]. The sparsity of the matrices directly determines the circuit complexity. State-space descriptions of filters with more zero elements require less hardware and are likely to consume lower power. Thus, it is therefore an important design aspect of state-space filters.

In respect to a fully optimized and fully dense state-space description, the resulting semi-optimal orthonormal filter structure differs only by about 2 dB in dynamic range. The A, B, and C matrices of the defined transfer function are as follows:

Matrix A:

0	2.60e10	0	0	0	0	0	0
-2.60e10	0	8.724e9	0	0	0	0	0
0	-8.724e9	0	2.572e10	0	0	0	0
0	0	-2.572e10	0	1.39e10	0	0	0
0	0	0	-1.39e10	0	2.513e10	0	0
0	0	0	0	-2.513e10	0	2.178e10	0
0	0	0	0	0	-2.178e10	0	3.933e10
0	0	0	0	0	0	-3.933e10	-4.704e10

Matrix B:

0	0	0	0	0	0	0	0	7.74e9

Matrix C:

-0.5779	-1.733	0.7325	0.0245	-0.1267	0.2073	0	0

C. *Scaling –capacitance and coefficient values*

Transconductance amplifiers will form the basic building blocks to implement the state-space description coefficients of the analog delay. The integrators are implemented as capacitors with a normalized value of 1 F. The corresponding matrices A, B, and C have extremely large coefficients corresponding to large gm values, which are not physically feasible at circuit level. By scaling the capacitors (cap=0.2 pF) and α_1, one consequently scales matrices A and B. Coefficients of matrix C can too be down scaled by α_2, without affecting the response of the filter.

$$\begin{aligned} A^* &= cap \cdot A \\ B^* &= \alpha_1 \cdot cap \cdot B \\ C^* &= \alpha_2 \cdot C \end{aligned} \tag{5}$$

The block diagram of the state-space filter is shown in Fig. 6 and has 22 non-zero coefficients.

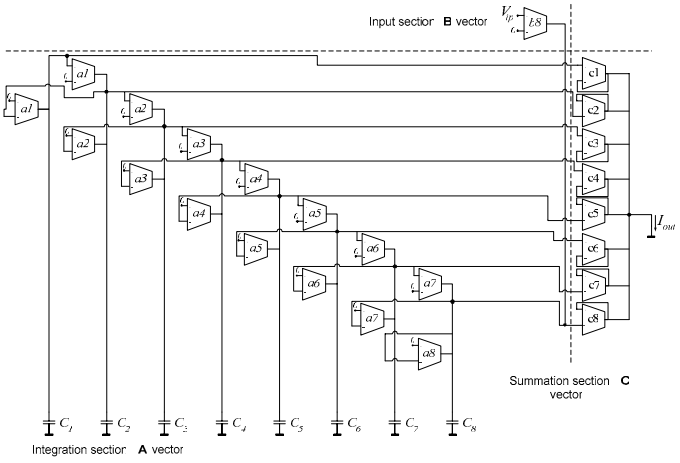

Fig. 6. Complete state-space filter structure

Once the block diagram has been recognized, a transconductance amplifier implements every coefficient.

IV. TRANSCONDUCTANCE AMPLIFIER

The transconductance amplifier is implemented using a negative feedback structure consisting of an active circuit, which implements a nullor and a feedback network (see Fig. 7). The nullor is an ideal network element that has infinite transfer parameters.

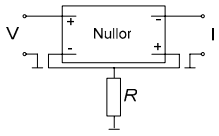

Fig. 7. Negative feedback amplifier

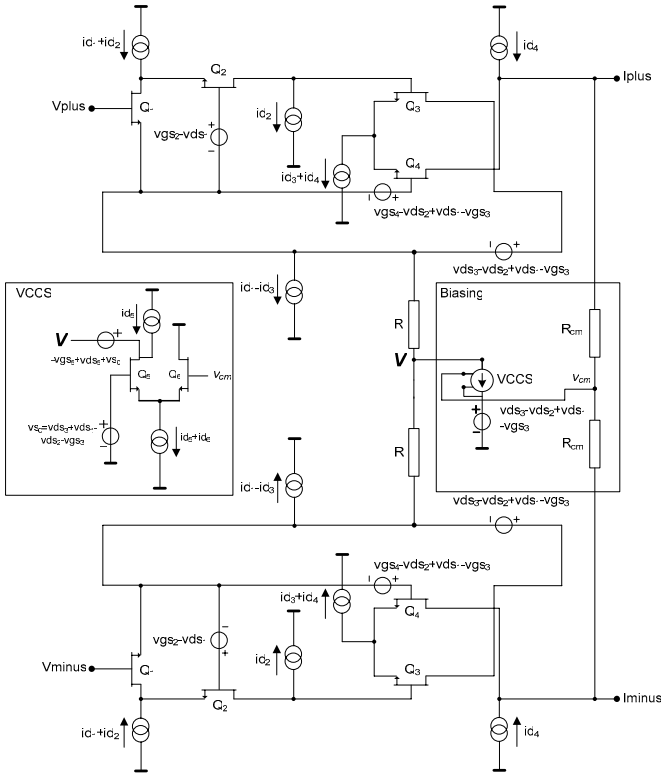

Fig. 8. 2-stage negative feedback gm amplifier

The orthonormal structure has both positive as well as negative coefficients. Since the structure in Fig. 7 can only implement a negative coefficient, a differential topology is used. Another advantage of using the latter is the cancellation of even order distortion terms may arise from the actual nullor implementation, thus improving linearity.

The nullor (half circuit) is realized using a cascode (*CS-CG*) stage formed by transistors (Q_1-Q_2) at the input, and a non-inverting cross-coupled differential pair (Q_3-Q_4) at the output. The feedback network is made up of a resistor ***R*** (see Fig. 8).

The CG-stage not only presents an output resistance that is larger by gm_2rds_2 but also reduces Miller's effect of the CS-stage [8]. As compared to a single-stage implementation, a 2-stage nullor improves the loop gain, which yields higher linearity as well as bandwidth [8] at the expense of power consumption. In reference to stability, frequency compensation in the form of pole-zero cancellation may be applied to this transconductance amplifier. For biasing of the differential structure, the common-mode voltage (v_{cm}) is sensed at the outputs by R_{cm} and is compared to the desired reference voltage using

a voltage-controlled-current source (*VCCS*). Its implementation is shown on the left hand side of Fig. 8. The output current delivered by the VCCS is then applied to a virtual ground node, *V*.

The small-signal behavior of the transconductance cell will now be analyzed.

A. Small-signal analysis

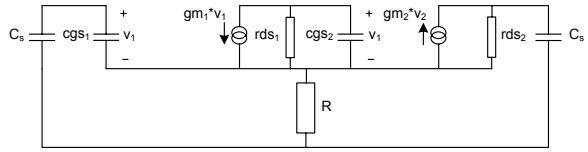

Fig. 9. Small signal model of the gm cell

For negative feedback amplifiers [8], the closed loop transfer (*At(s)*) can be written in terms of the loop gain *Aβ(s)* as,

$$At(s) = -\xi \cdot \nu \cdot At_{\infty} \cdot \left[\frac{-A\beta(s)}{1 - A\beta(s)}\right] \tag{6}$$

where ν and ξ represent the input and output coupling factors and both are assumed to be equal to one.

At_{∞} is defined as,

$$At = -\frac{1}{\beta} \tag{7}$$

where β is the feedback transfer. Now $A\beta(s)$ can be expressed as,

$$A\beta(s) = -gm_1 \cdot gm_2 \cdot \left[\frac{rds_2}{rds_2 + \frac{1}{sCs} + \left(R // \left(\frac{1}{s(cgs'_1)}\right)\right)}\right] \cdot \left[\frac{R}{R + \frac{1}{s(cgs'_1)}}\right] \cdot \left[\frac{rds_1}{1 + s(rds_1 \cdot cgs_2)}\right] \cdot \frac{1}{s(cgs_1)} \tag{8}$$

$$cgs'_1 = \left[\frac{cgs_1 \cdot Cs}{cgs_1 + Cs}\right] \tag{9}$$

where gm_1 and gm_2 are the transistor transconductances of the CS-stage and the differential pair, respectively, rds_1, cgs_1 and rds_2, cgs_2 are the drain-source resistances and gate source capacitances of Q_1 and $Q_{3\text{-}4}$, respectively and R is the feedback resistance. The integrating capacitors (*Cs*) at the input and output have also been taken into account. Note that for high frequencies, the zero at the origin as a result of the source *Cs* will be neglected.

Simplifying by substituting (9) in (8), one obtains,

$$A\beta(s) = -gm_1 \cdot gm_2 \cdot \left[\frac{rds_2}{rds_2 + R}\right] \cdot \left[\frac{R}{1 + sR\left(\frac{Cs \cdot cgs_1}{Cs + cgs_1}\right)}\right] \cdot \left[\frac{rds_1}{1 + s(rds_1 \cdot cgs_2)}\right] \cdot \frac{Cs}{Cs + cgs_1} \tag{10}$$

Substituting (10) in (6) and for large enough loop gains, the transfer is accurately determined by the feedback transfer β.

$$At = -\frac{1}{R} \cdot \left[\frac{-A\beta(s)}{1 - A\beta(s)}\right] \approx -\frac{1}{R} \tag{11}$$

The DC loop-gain-poles product (LP_2) predicts the bandwidth of the system and equals [8],

$$LP_2 \approx |A\beta(0)| \cdot |p_1| \cdot |p_2| \tag{12}$$

Substituting dc loop gain $A\beta(0)$ (13), closed loop poles p_1 and p_2 ((14) and (15), respectively) in (12),

$$A\beta(0) = -gm_1 \cdot gm_2 \cdot \left[\frac{rds_2}{rds_2 + R}\right] \cdot rds_1 \cdot R \tag{13}$$

$$p_1 = \left[\frac{-1}{2\pi(rds_1 \cdot cgs_2)}\right] \tag{14}$$

$$p_2 = \left[\frac{-1}{2\pi R\left(\frac{Cs \cdot cgs_1}{Cs + cgs_1}\right)}\right] \tag{15}$$

the bandwidth, *BW*, of the proposed 2-stage transconductance amplifier is approximately equal to the geometric mean of the transit frequencies of the respective stages [8], assuming that $r_{ds2} >> R$.

$$LP_2 \approx f_{T1} \cdot f_{T2} \rightarrow BW \approx \sqrt{LP_2} \approx f_T \tag{16}$$

The influence on the transfer by the non-ideal coupling at the input and output modeled via (ξ) and (ν) [8], respectively, needs to be taken into account. This aspect will result in a *BW* to some extent lower than f_T. The gm-C topology is implemented in IBM's 0.12 µm CMOS technology. In the same technology, the current sources in Fig. 8 are implemented using current mirrors with multiple outputs. The voltage sources are implemented using voltage buffers.

V. SIMULATION RESULTS

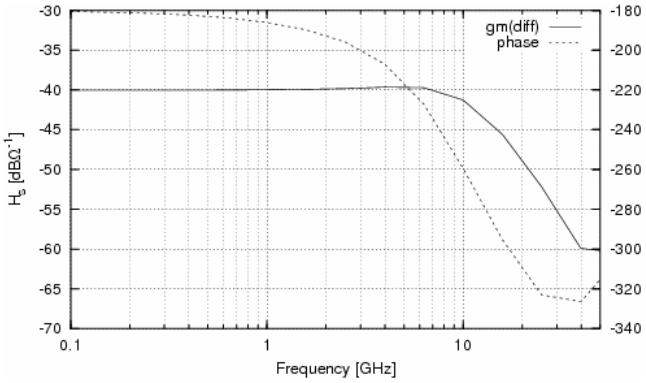

Fig. 10. Magnitude and phase transfer of stand-alone gm cell

Fig. 10 shows the magnitude and phase response of the stand-alone transconductance amplifier, which is used in this filter. Both the magnitude and the phase demonstrate a relatively flat response up to about 3 GHz.

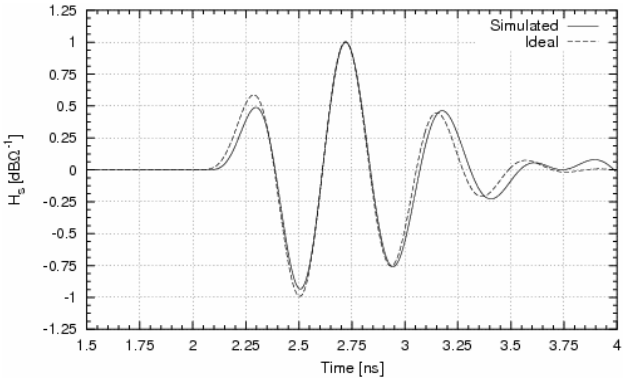

Fig. 11. Impulse response of an 8th order Morlet filter centered at 2.2 GHz

The simulated impulse and the phase response of the Morlet filter are seen in Fig. 11 and Fig. 12., respectively. By scaling down the capacitance even lower than 0.2 pF as well as the coefficients in the matrices *A* and *B*, smaller pulse widths are attainable because of the trade-off between bandwidth and gain.

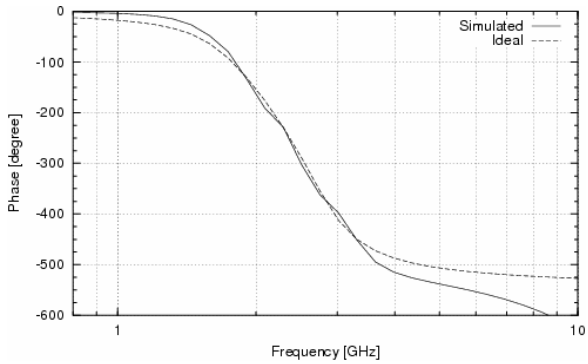

Fig. 12. Ideal vs. simulated phase response

Fig. 13. shows the time delay (τ) between the Morlet waveform and the convolved signal. In addition, the impulse response it taken at 2 ns.

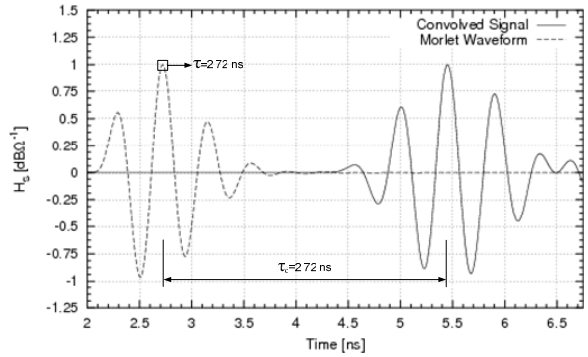

Fig. 13. Time delay between the incoming Morlet waveform and convolved signal

Finally, by randomly varying (i.e. 5 iterations) the component tolerances as well as the model parameters between their specified tolerance limits, a Monte Carlo analysis is run in order to estimate the circuit's sensitivity. From Fig. 14 it is inferred that the time delay is relatively unlikely to show discrepancy as a result of neither process variations nor component mismatches.

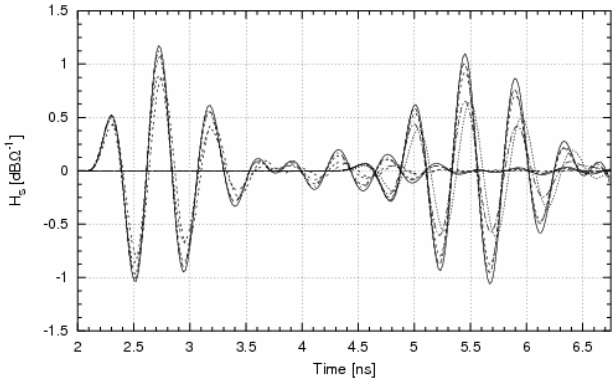

Fig. 14. Monte Carlo – (left) impulse response and (right) convolved waveform

The simulation parameters of the delay filter are given in Table I.

TABLE I
SIMULATION PARAMETERS

Specifications	Simulated (@ 1GHz)
1-dB compression pt. at	565 mV
Dynamic range at 1-dB compression pt. (SNR)	+47.5 dB
Time delay (τ)	0.72 ns
Current consumption	70 mA @ 1.6 V
Size	1.25 mm^2
Process	IBM CMOS 0.12 µm

VI. CONCLUSIONS

A frequency selective analog delay, which is to be used in the QDAR, has been presented. An eighth order Padé approximation of the delay transfer function is selected. Subsequently, an orthonormal state-space approach is adopted, which fulfills the requirements of dynamic range, sensitivity, and sparsity. The coefficients are down scaled in conjunction with capacitance values. Each element of the delay is implemented at circuit level using a novel negative feedback 2-stage gm amplifier. Simulation results in IBM's CMOS 0.12 µm technology (see Table 1) show that the delay requires a total current 70 mA at a 1.6 V power supply. The 1-dB compression point of the delay is at 565 mV and the SNR is 47.5 dB.

VII. REFERENCES

[1] S.A.P. Haddad, S. Bagga and W.A. Serdijn, "Log-Domain Wavelet Bases," in *Proceedings IEEE International Symposium of Circuits and Systems*, May 2004

[2] R.T. Hoctor and H.W. Tomlinson, "Delay-Hopped Transmitted-Reference RF Communications," *Proceedings of the IEEE Conference on Ultra Wideband Systems and Technologies*, pp. 265-270, May 2002

[3] S. Bagga, S.A.P. Haddad, Koen van Hartingsveldt, Simon Lee and W.A. Serdijn, "An Interference Rejection Filter For An Ultra-Wideband Quadrature Downconversion Autocorrelation Receiver," in *Proceedings IEEE International Symposium of Circuits and Systems*, May 2005

[4] Simon Lee, S. Bagga and W.A. Serdijn, "A Quadrature Downconversion Autocorrelation Receiver Architecture for UWB," Joint *UWBST and IWUWBS*, May 2004

[5] D. Rocha, "Optimal Design of Analogue Low-Power Systems: A strongly directional hearing-aid adapter," PhD Thesis, Delft University of Technology, 2003

[6] D.A. Johns, W.M. Snelgrove and A.S. Sedra, "Orthonormal Ladder Filters," *IEEE Transactions on Circuits and Systems*, vol. 36, pp. 337-343, March 1989

[7] G. Groenewold, "*Optimal dynamic range integrators*", IEEE Transactions on Circuits and Systems, Volume: 39, Issue: 8, Aug. 1992, Pages: 614 - 627

[8] C.J.M.Verhoeven, A. van Staveren, G.L.E. Monna M.H.L. Kouwenhoven and E. Yildiz, "Structured Electronic Design: Negative-Feedback Amplifiers", Kluwer Academic Publishers, 2003